A μ-Synthesis Based Control for Compliant Maneuvers

Yutaka Uchimura
Kajima Technical Research Institute,
Tobitakyu, Chofu-shi,
Tokyo 182, Japan
e-mail: yuchi@kajima.com

H. Kazerooni
Mechanical Engineering Department,
University of California at Berkeley,
Berkeley, CA 94720
e-mail: kazerooni@berkeley.edu

This paper deals with a system, which is subjected to very uncertain factors: human and environment. These independent uncertainties are dealt with explicitly on the framework of μ-synthesis. We also describe a controller design, which enables a robust force feedback without using a force sensor. The model of human dynamics, environments, and actuators are modeled associated with uncertainties described in the form of weighting functions. A controller is designed based on the μ-synthesis so that it maintains robust performance against uncertainties in both environment and human dynamics, which contributes to dexterous manipulation. The controller described here is implemented on the human power extender, which is worn by a human and amplifies the human's physical strength, while the human's intelligence remains as the central control system for manipulation. Experimental results conducted on the extender showed that the force estimation worked fine and the control system performed as desired. [DOI: 10.1115/1.2362810]

1 Introduction

Recently, with the progress of computers, robot manipulators have obtained some abilities of perception and judgment. However, it still remains a dream that robots have the same or more flexible intelligence than humans. In the mean time, the physical ability of a robot manipulator is superior in cases such as carrying heavy loads. To benefit from the physical advantage of robots and the intellectual advantage of humans, the human extender was studied [1].

The human power extenders are a class of robots, which are worn by a human and amplify the human's physical strength, while the human's intelligence remains as the central control system for manipulation. The human transfers his/her commands to the extender via the contact forces between the human and the extender. For the sake of better dexterity, the extender should also transfer to the human a scaled-down value of the actual external forces, and then the human "feels" them during manipulations. To achieve this, the force, which interacts between the environment and the extender, has to be sensed.

A force sensor is the typical answer, but extracting the external force may be possible only when the exact model of the system is obtained. Due to the existence of nonlinearities or unmodeled dynamics, the exact model may not be obtained. But it can still be beneficial to let the human operator feel the interactive force as long as the estimated force maintains some degree of accuracy. For this reason, we develop an algorithm, which estimates the external forces using input voltage to the actuators and output position from encoders. This force information feeds back to the operator at some scaled down ratio. In other words, the operator's force is amplified in accordance with this ratio. The ratio should maintain the same value as long as the task is the same. This is one of the goals for designing an extender control system.

Meanwhile, the control system is subjected to many uncertainties such as human dynamics and unknown environments. The extender must be stable against these various uncertainties. In fact, the performance goal of maintaining the force amplification ratio and stability against uncertainties contradicts each other. Therefore we must design the controller using a criterion, which optimizes this trade-off. μ-synthesis is one of the most powerful theories especially for systems, which involves independent uncertainties. To take advantage of it, the controller was designed based on this theory.

Section 2 describes the modeling of the extender system and states the problem, which concerns the stability and performance. It also discusses the modeling of the human arm. In Sec. 3, we discuss an algorithm to estimate an external force without a force sensor. It also discusses viscous friction at low frequencies and static friction that deteriorates the accuracy of the estimation. Section 4 presents the controller design procedure and experimental results.

2 Modeling of the System

The whole dynamics of the human power extender is coupled with the dynamics of the human, environment, and the actuator, which are combined in Fig. 1. The system mainly involves two loop systems: the human dynamics loop and environmental loop. The upper half of Fig. 1 represents the human dynamics loop, which includes the force produced by the human arm impedance, H_m and intentional forces generated by human's nerve system. The latter force, u_h, is a source for maneuvering the actuator. The force imposed on the actuator, f_h, is the difference between these two forces, which is measured for the controller.

The lower half loop represents the dynamics of the environment. It is produced as a result of interaction with the external environment such as contact forces or gravity forces due to the weight of a load. The force, f_e, generated by the impedance of the dynamics, E_n, is also imposed on the actuator. This force is to be estimated by the algorithm, which is described in a later section.

2.1 Performance. Maneuvering the human arm from one point to another point can be a position servo problem. However, it is impossible to measure the exact position in 3D space where a human would like to move his arm in the next moment. The only thing we can do is to measure the force difference between the human's intentional force and the resistance force due to impedance of the human. At the moment when the human does not want to move his/her arm, zero signals come out. One possible design method of the controller is to place a double integrator whose initial state is a starting position, then input the integrated signal to the position servo controller. However, this should be avoided because the controller is to be implemented on a digital computer. Converting from continuous time integrator to discrete time will result in an integration error.

Another possible solution is to consider the system as a regulator problem. Now we define the performance of the system; to

Contributed by the Dynamic Systems, Measurement, and Control Division of ASME for publication in the JOURNAL OF DYNAMIC SYSTEMS, MEASUREMENT, AND CONTROL. Manuscript received February 1, 2004; final manuscript received April 12, 2006. Assoc. Editor: Reza Langari.

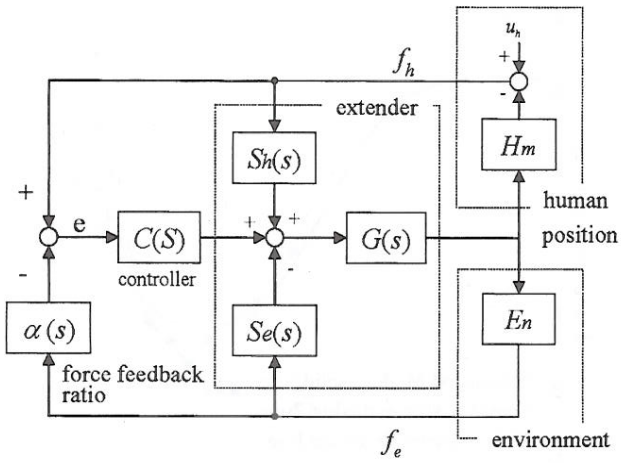

Fig. 1 The overall block diagram for the extender

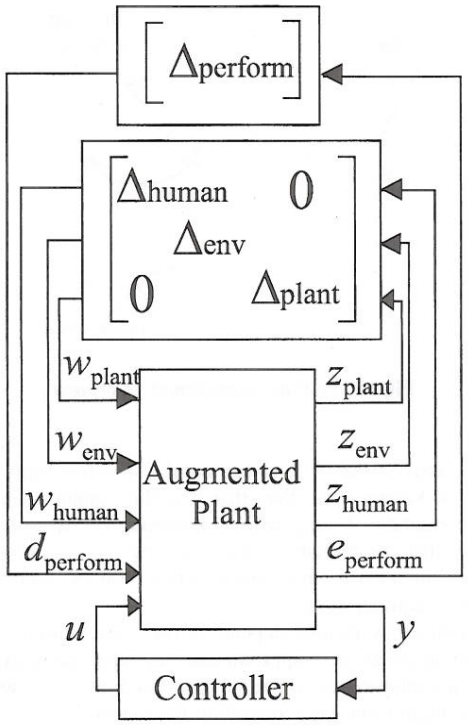

Fig. 2 Framework for μ based control design

minimize the human's force measured by a sensor. The controller works to keep the measured force zero, which causes the actuator to move along with the human motion. This design scheme is more preferable and has better performance.

Without any interaction with an environment, the specification of the system design is to let the actuator move along with human motion without stress. This will be achieved by attenuating disturbances existing in the actuator such as friction. However, once the actuator comes into contact with the external environment, such a performance goal sometimes leads to an unexpected result. Pushing a pin into a hole is a well-known example. Under a constrained environment, the human needs to feel the interaction effect from the environment.

The force feedback ratio α in Fig. 1 takes such a role in the system, which lets designers choose the appropriate performance for the actuator. The larger α is, the more the human feels the interaction; α signifies the human power amplification. In order to maintain the power amplification performance, the magnitudes of f_h and αf_e in Fig. 1 needs to be sufficiently close to each other in the presence of disturbances that are bounded in magnitude and frequency. The goal is to decrease the undesirable effect of disturbances on the difference between f_h and αf_e. This is framed mathematically by defining a sensitivity transfer function representing the difference between f_h and αf_e. The goal is to minimize the norm of this sensitivity transfer function within a bounded frequency range.

2.2 System Design Based on μ-Synthesis. Exact dynamic models for the system are difficult to produce because of uncertainties in the human dynamics, environments, and the actuator. The human arm dynamics change with each human and also in one person over time. Moreover, unmodeled dynamics also involves nonlinearly. Uncertain environment may change even more drastically, because the extender has to always be stable both with and without contact. The stiffness of the environment may change from nothing to a very large value. Such perturbations cannot be negligible nor be dealt with as unmodeled disturbances.

Several studies about the extender's stability had been made based on small gain theory and derived a sufficient condition [1,2]. They also deal with performance of the system. However, they just show a sufficient condition for the performance and stability.

H_∞ synthesis may be a solution for the theoretical procedure of designing a controller. However it will just design a very conservative, sufficient controller for the extender system, which has multiple uncertainties. One of the main reasons is that the uncertainty of human and environment are independent. These uncertainties should be dealt with separately, i.e., these are to be represented as a structured singular value [3–5].

A μ-synthesis can deal with such a system that has multiple independent uncertainties and designs a controller that maintains robust performance in the face of plant uncertainties.

The framework for μ-synthesis based control design is illustrated in Fig. 2, where Δ represents the uncertainties on the system due to parameter variations in dynamics of the human and the environment and unmodeled dynamics of the plant. The inputs and outputs corresponding to the uncertainties in the system are w and z, respectively.

The input vector, d_{perform}, denotes all external disturbances acting on the plan. The output vector e_{perform} contains the regulated performance variables. Feedback measurements are denoted by the vector y, and u represents the control vector that is the input to the plant actuators.

Associated with the weighting function, the norms of Δs are normalized and the performance of the system can be represented as perturbation as well as other uncertainties, whereas they are dealt with separately. For the augmented system with perturbations, the system is stable as long as the structured singular value μ remains at less than 1. However, it is difficult to compute the structured singular value analytically [6], therefore we employed the D-K iteration method to obtain the upper and lower value of the structured singular value. In the actual system design of the extender, these two values were very close, which means that the structured singular value was numerically converged, thus the obtained controller was one of the suboptimal controllers. Controller design procedure is described in a later section.

2.3 Modeling of the Human Arm. This subsection describes the dynamic behavior of the human arm. A simplified version of human arm dynamics is already shown in Fig. 1. The force imposed by the human arm on the extender results from two inputs. The central nervous system and the motion of the extender issue the first input and the second input. These two forces can be translated as active force and passive force, respectively. If the extender is stationary, the force imposed on the extender is only from the active force. However, if the extender moves, the force imposed on the extender is not only from the active force but also

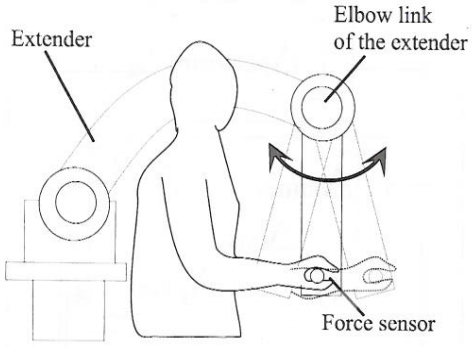

Fig. 3 Human experiment overview

from the passive force. It assumed that the specified form of active force is not known other than that it is the human's intention to move the extender. It may help to illustrate the passive force by imagining that the human is sleeping. The passive force is produced by human arm impedance, which can be modeled as a spring-mass-damper system.

The model may change depending on configuration; therefore the model delivered here approximates an experimentally verified model at a configuration in the neighborhood of Fig. 3, which is a typical configuration when operating the extender.

For the experiments, an examinee's hand was placed on the grip connected on the force sensor, and then the extender was moved along the sinusoidal velocity command. The maximum magnitudes of sinusoidal commands had been set to the same value. Figure 4 shows experimental results of male and female examinees. The horizontal axis is the frequency of velocity (rad/s). The vertical axis is the magnitude of the measured force in dB form (N s/m). At low frequency, the spring factor is dominant and the middle convex part represents the dumping coefficient. The inclining curve at high frequency is due to mass effects. By applying the least squares method on the data at each frequency, damping and mass were obtained with small standard deviations. However, spring was not. These results show that the human spring factor does not have a linear aspect; even so it must have a certain limited value. To estimate the maximum value of the spring factor, we conducted a simple third order force feedback system composed of the actuator and first order force sensor. In this system, only the spring factor may destabilize the system. In this experiment, the examinee just holds the bar, then we increase the proportional gain. At the limit of gain or phase margin the system goes unstable.

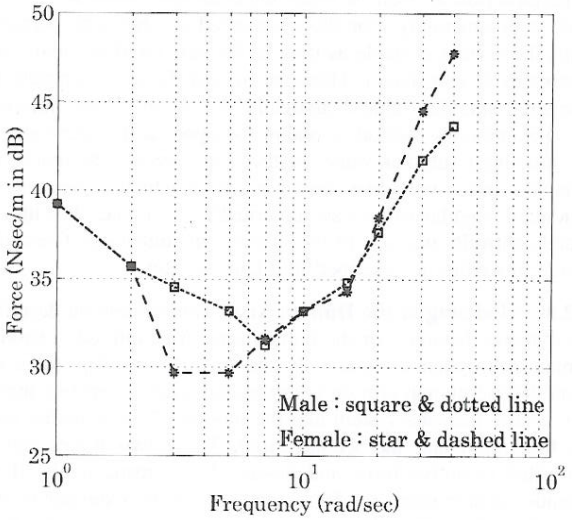

Fig. 4 Experimental results on human arm

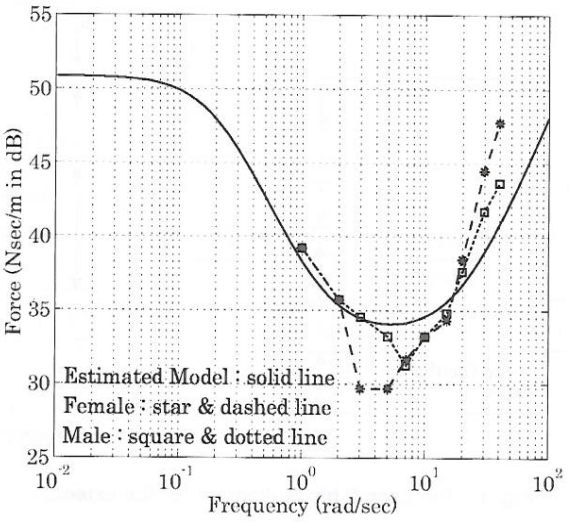

Fig. 5 Frequency response of the nominal model

Based on several experiments, the best estimate for the nominal model of a human's arm dynamics is presented as Eq. (1). Figure 5 shows the frequency response of H_m/s,

$$H_m = 2.5s^2 + 50s + \frac{60s}{s+0.2}(\text{N/m}) \tag{1}$$

3 Estimation of the External Force

3.1 The Estimation Procedure. For simplicity, we discuss only one of the links of the extender, whose block diagram is depicted in Fig. 6.

Notations are as follows: u is input voltage to the motor, i is current, K_t is torque coefficient, N is a speed reduction ratio, τ is the torque, D is viscous friction, J is the inertia both of the link and the motor, L is the inductance, R is the resistance, and q is the rotational angle.

dis stands for disturbances which are not defined explicitly in the block diagram such as Coulomb frictions, Coriolis, centrifugal forces, external forces, and model uncertainties.

Coriolis and centrifugal forces are negligible when N is large enough. Also L is very small compared to R, hence we can approximate the dynamics of the link as

$$Eu = J\ddot{q} + D\dot{q} + Mg\sin q + C\,\text{sgn}(\dot{q}) + F_{\text{ex}} \tag{2}$$

where $E=KtN/R$, J is the inertia, $Mg\sin q$ is the gravitational torque, and C is the Coulomb friction.

Now we define a vector $\mathbf{X}=[J\ D\ Mg\ C]^T$ and $\mathbf{A}=[\ddot{q}\ \dot{q}\ \sin q\ \text{sgn}(\dot{q})]$. Equation (3) can be rewritten

$$Eu = \mathbf{AX} + F_{\text{ex}} \tag{3}$$

$\ddot{q}$, $\dot{q}$, $\sin q$, and $\text{sgn}(\dot{q})$ can be numerically calculated from the measurement set of u and q as a sequence of time responses.

In practice, measured data should be filtered to maintain quality against noise. Therefore (3) is rewritten associated with noise,

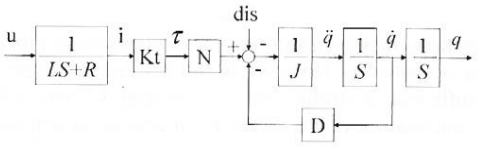

Fig. 6 Dynamics of a link

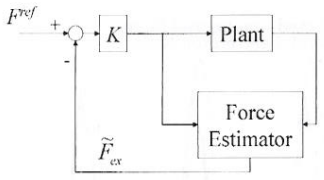

Fig. 7 Force servo control system

$$Eu^* = \mathbf{A}^*\mathbf{X} + F_{ex}^* + \omega \tag{4}$$

where u^*, $\mathbf{A}^*$, F_{ex}^* are filtered values and ω is noise. Since E can be known from the specification of motor or experimental analyses, $\mathbf{X}$ can be estimated by $\mathbf{A}^*$ from the measurement data when $F_{ex}^*=0$. Numbers of the least square mean method algorithms were already studied and had come into wide use [7]. Among them, we used Potter's algorithm, which turned out to be more accurate and stable than Kalman by experiments.

Once the external force works on the manipulator, subjected external force $\hat{F}_{ex}$ is estimated as

$$\hat{F}_{ex} = Eu^* - \mathbf{A}^*\hat{\mathbf{X}} \tag{5}$$

where $\hat{\mathbf{X}}$ is the estimated parameter vector.

3.2 Frictions at Low Velocity. In the practical system, position is obtained from an encoder, which gives quantized (digital) values. This causes a numerical differential operation to generate jaggy oscillations along $\mathrm{sgn}(\dot{q})=0$ and the Coulomb friction term $C\,\mathrm{sgn}(\dot{q})$ switches between $-C$ and C at very high frequency. As a result, estimated external force will be corrupted and intolerable with noise. To avoid this, we implement an insensitive area for the sgn function by replacing it with the following function $s\omega(\dot{q})$:

$$s\omega(\dot{q}) = \begin{cases} 0 & |\dot{q}| < \delta \\ \mathrm{sgn}(\dot{q}) & |\dot{q}| \geqslant \delta \end{cases} \tag{6}$$

where $\delta>0$ determines the range of insensitivity.

At the moment when velocity is zero, a static friction arises instead of Coulomb friction.

Even though the maximum magnitude of the static force is known, the static force cannot be estimated accurately, because the static friction changes in accordance with the sum of all other forces. If $\dot{q}$ is zero, the static friction force F_s is defined as

$$F_s = -Eu + Mg\sin q + F_{ex}; \quad |F_s| \leqslant F_s^{\max} \tag{7}$$

Therefore the estimated external force based on the procedure described above may have an error bounded by $|F_s^{\max}|$.

Now suppose a force servo control system as shown in Fig. 7. When $F^{ref}=0$, the actuator is required not to move. However, F_{ex} is not always zero due to the estimation error. As a result, the link will start to move.

Essentially, what we proposed is to construct the estimation of system dynamics. Static friction can be modeled as a dead zone depicted in Fig. 8. Therefore, we also need a dead zone located at

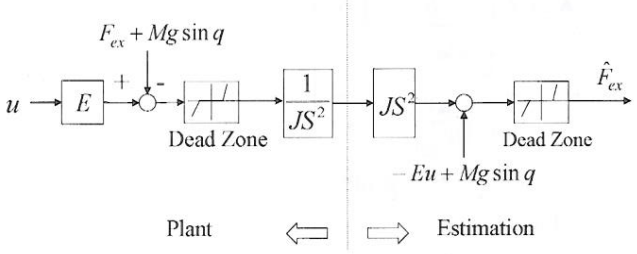

Fig. 8 External force estimation via dead zone

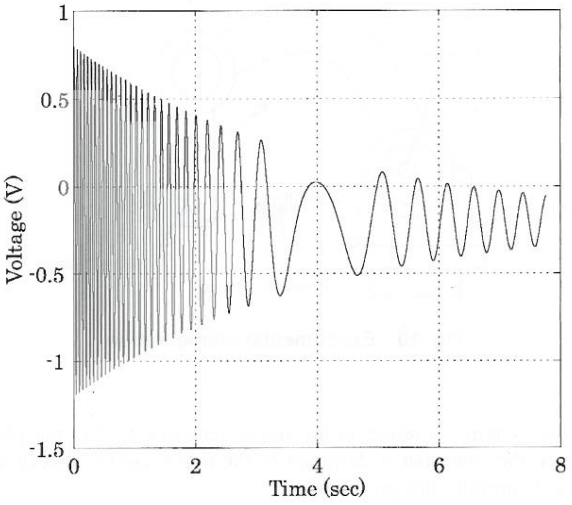

Fig. 9 Input signal for identification

the end of the estimation of the system.

The revised estimation algorithm when $s\omega(\dot{q})=0$ is shown in (8),

$$F_{ex} = \begin{cases} -F_m & |F_m| > F_s^{\max} \\ 0 & |F_m| \leqslant F_s^{\max} \end{cases}$$

$$F_m = Eu + Mg\sin(q) \tag{8}$$

3.3 Experimental Results

3.3.1 Model Identification. The experiments are conducted using the last link (elbow link) extender. We executed identification with various input command signals into the actuator. Among them, a chirp signal with dc offset was expected to be most reliable, because they contain contributions from a specified frequency range. The signal possesses (nearly) uniform frequency components between 0 (rad/s) and 100 (rad/s). A time response plot of the signal appears in Fig. 9. The result of identification is shown in Table 1.

Both input and output data (value of encoder) were stored in the memories of the host computer every 1 ms and used for the parameter identification. The data obtained from the encoder was transformed into the rotational angle of the link and one of the axes of the coordinate was calibrated to the direction of gravity. As descried in Sec. 3.1, we used Potter's algorithm and the final value of recursive execution was adopted as estimated values.

3.3.2 Estimation of External Force. In order to verify the reliability of identified dynamics, we conducted experiments as shown in Fig. 10. The external force is emulated by a tension spring which is connected between the base of the extender and the end of the elbow link. The actuator is controlled to follow a sinusoidal velocity command, while stretching the spring.

Figure 11 shows the experimental result. The magnitude of estimated force is fairly accurate, while a phase delay is observed. The low pass filtering used in the force estimation process causes the phase delay. Excessive delay will cut out the stability margin

Table 1 Identified parameters

J (N ms^2/rad)	D (N ms/rad)	C (N/m)	Mg (N m/rad)
4.48	23.2	14.54	35.01

[a] KtN/R=118 Nm/V

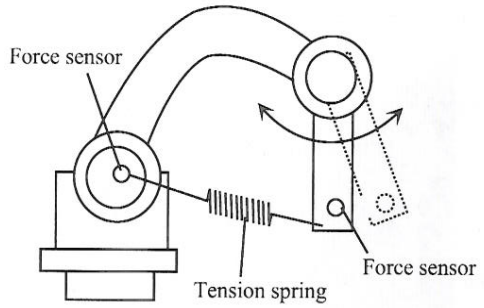

Fig. 10 Experimental configuration

of the system, therefore in the implementation to the real plant, even if the controller is designed by the robust control theory, one should carefully design the filter.

4 Controller Design and Experimental Verification

4.1 Controller Design. The block diagram of the closed loop system is shown in Fig. 12. In the figure, Wx denotes a weighting function and Hx denotes a parameter of a human dynamics, where the suffix x corresponds to each block in the diagram. d_x is a disturbance input to the augmented plant and e_x is the associated output, which are used for the performance measure. w_x is a perturbation input and z_t is the associated output, which are used to represent uncertainties. The closed loop system includes the feedback structure of elements associated with the uncertainty models and performance objectives. The design objective of the controller is to maintain the desired performance against uncertainties of actuator, human, and environmental dynamics while optimizing performance.

4.2 Nominal Models and Uncertainties

4.2.1 Actuator. Nominal model of the actuator is derived from the result of identification, which is described in Sec. 3

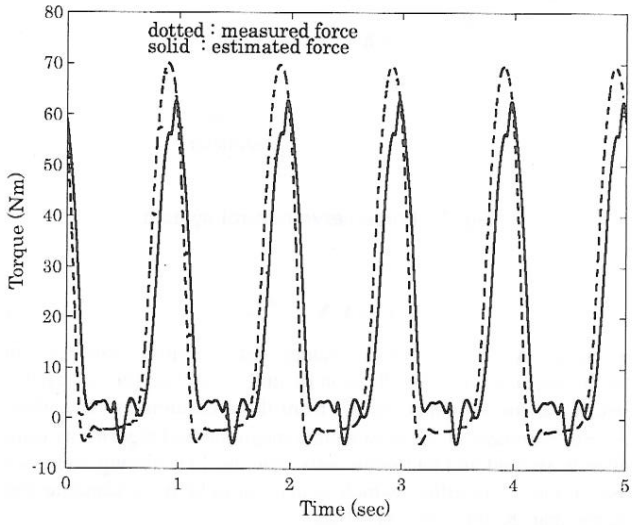

Fig. 11 Estimation results

$$P_m(s) = \frac{26}{s(s+6)} \tag{9}$$

Uncertainty of the actuator was modeled as a multipicable uncertainty with a weighting function, which is chosen as follows. The gain plot is shown in Fig. 13,

$$W_t(s) = \frac{100s^2 + 84000s + 3.6 \times 10^7}{s^2 + 26560s + 3.6 \times 10^8} \tag{10}$$

The uncertainty weight chosen indicates that at low frequencies there is potentially a 10% modeling error, and at high frequencies the model is up to 100 times larger than the nominal model.

4.2.2 Human Dynamics. Nominal model of human dynamics is derived from the experimental analysis in Sec. 2

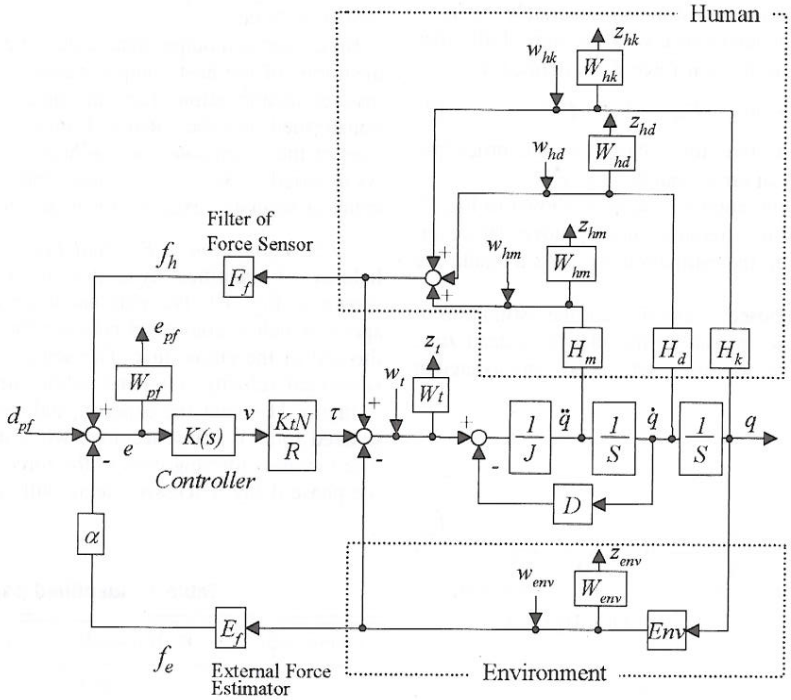

Fig. 12 Block diagram with weighting functions

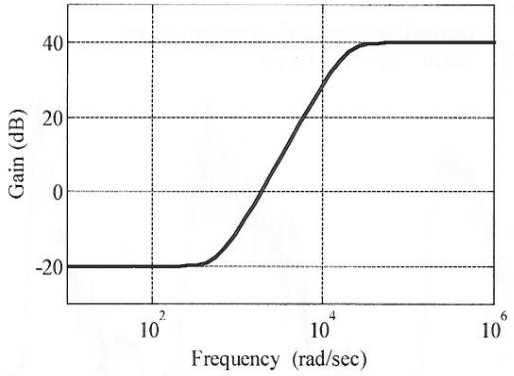

Fig. 13 Gain plot of the weighting function *Wt*(s)

$$H_{\text{nominal}}(s) = H_{mn}s^2 + H_{dn}s + H_{kn} \tag{11}$$

where H_{mn}=2.5 N s^2/m, H_{dn}=50 N s/m, H_{kn}=60s/(s+0.2) N/m.

Uncertainty of the human is modeled as multiplicable real parametric perturbations. To normalize the perturbation, the weights are chosen as 0.2, 0.3, 0.3, which indicate that the human's mass, damper, and spring may change 20%, 30%, 30%, respectively. With these perturbations, the perturbed model almost covers the upper bounds of human dynamics shown in Figs. 4 and 5.

4.2.3 Environment Dynamics. Nominal environment is modeled as a spring system. Uncertainty is modeled as a multiplicable complex parametric perturbation whose weight is 1. This assumes the stiffness of the environment will perturb 0–200% of the nominal value. One should need to notice that complex parametric perturbation assumes that the environment also has a damper whose magnitude will also perturb. Because a complex uncertain parameter is mathematically equivalent to robustness, the Nyquist plots lie in the disks. Suppose the nominal stiffness of the spring is 5000 N/m, the system can exist within the circle with center at 5000 N/m and radius 5000 N/m.

4.2.4 Robust Performance. As discussed in Sec. 2.1, the control objective is to force f_h and αf_e to be sufficiently close to each other, in the presence of disturbances. The main source of disturbances (represented by d_{perf} in Fig. 12) is unexpected external forces imposed on the extender arm. For example, when the extender makes a hole on a target environment using a hammer, the hammer generates impact forces which negatively affects the extender arm. Such disturbances are intermittent and decay by time, thus the L_2 norm of d_{perf} can be assumed to be finite, i.e., $d_{\text{perf}} \in L_2$. To attenuate the undesirable effect of d_{perf} on e, one approach is to force the gain of the transfer function T_{pf}, from d_{perf} to e, to be small. This can be done by designing a controller that reduces $\|T_{pf}\|_\infty$.

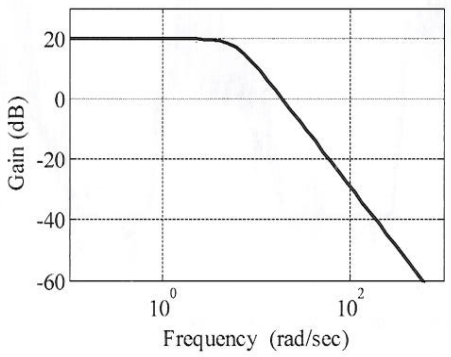

Fig. 14 Gain plot of the weighting function W_{pf}(s)

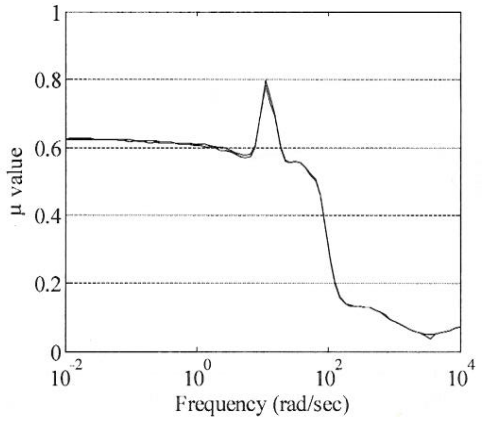

Fig. 15 Upper and lower bounds of μ

Considering an appropriate weighting function, $W_{pf}(s)$, the performance is guaranteed if $\|W_{pf}T_{pf}\|_\infty < 1$ is satisfied. W_{pf} (s) is chosen to have a large gain at low frequencies and smaller gain at higher frequencies in order to cover the frequency range of human's arm maneuvers. This weighting function also characterizes the attenuation of disturbance. A feasible choice of W_{pf} (s) is shown by Eq. (12) and its gain is plotted in Fig. 14.

$$W_{pf}(s) = \frac{360}{s^2 + 8.48s + 36} \tag{12}$$

As previously stated, the system has uncertainties and transfer function T_{pf} is not fixed to a nominal model. To assure a robust performance in the presence of all uncertainties, $\|W_{pf}T_{pf}\|_\infty < 1$ needs to be satisfied for all possible perturbed T_{pf}.

4.2.5 Filters. There are two filters in the system to attenuate noise at the high frequency. One is the filter for the force sensor, which measures the human's force. The other one exists in the external force estimation.

The filter for the force sensor is chosen as second order Butterworth filter whose cutoff frequency is 50 rad/s.

The force estimation uses numerical derivatives to obtain acceleration and velocity associated with low pass filters. These filters

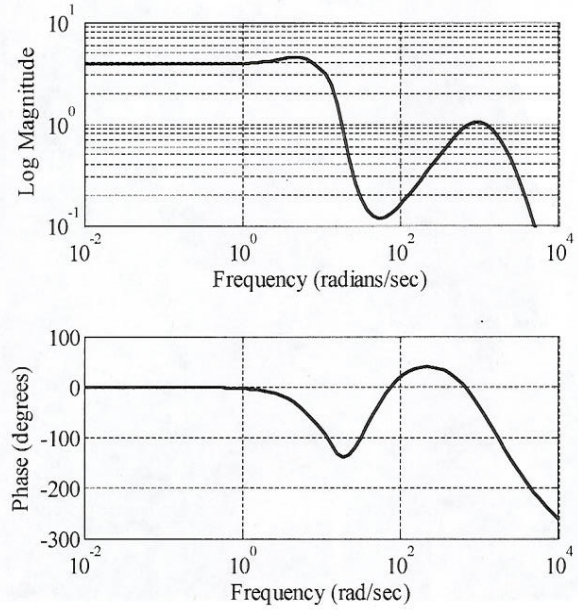

Fig. 16 Bode plot of the reduced order controller

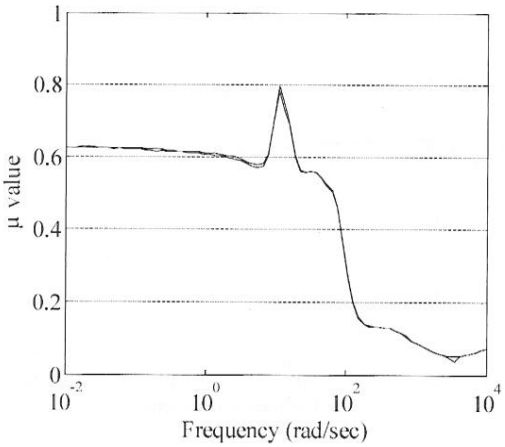

Fig. 17 μ plot with the reduced order controller

are also applied to other elements. Therefore total filter order is the fourth order low pass filter, which is chosen as

$$E_f(s) = \frac{1}{(1/50s+1)^4} \tag{13}$$

Because these filters are digital filters on the host computer of the extender, we therefore assume no uncertainty.

4.3 Computation of Controller and Trade-Off Between Stability and Performance. Performance is strongly affected by the uncertainties of the plant. In the case of the extender model, the uncertainty of the environment restricts performance most significantly. For this reason, we had to compromise either performance or maximum stiffness of the environment. Such trade-off depends on the purpose of using the extender. In our study, the reasonable problem statement is:

Achieve less than 10% error for the environment whose nominal value is 12,500 N/m, and it may change from 0 to 25,000 N/m.

The controller is obtained using D-K iteration methods, whose maximum D-scale state order is 5. After 4-time D-K iterations, a 53rd order controller is obtained which achieves a structured singular value μ is less than 1. Figure 15 shows the frequency response of the upper and lower bounds for μ.

For the experimental implementation, the controller order was reduced to 12th order using truncated balance realizations. The reduced order controller still maintains closed-loop stability and robust performance. Figure 16 shows the Bode plot of the controller and Fig. 17 shows the μ plot of the reduced order controller.

4.4 Experimental Results. The prototype three-degree of freedom electrical extender (Fig. 18) is used to verify the stability and performance of the controller implemented system. For the experiment, only the last link from the base (the elbow link) was used. A piezoelectric force sensor for measuring the human force is installed near the end of the link. The actuator of the link is composed of a dc brushless motor and a harmonic drive gear with a reduction ratio of 50:1. To emulate the environment two test pieces were employed: a tensional spring whose stiffness is about 4000 N/m and a metal wire whose stiffness is around 20,000 N/m. Either of them is set between the base of the ex-

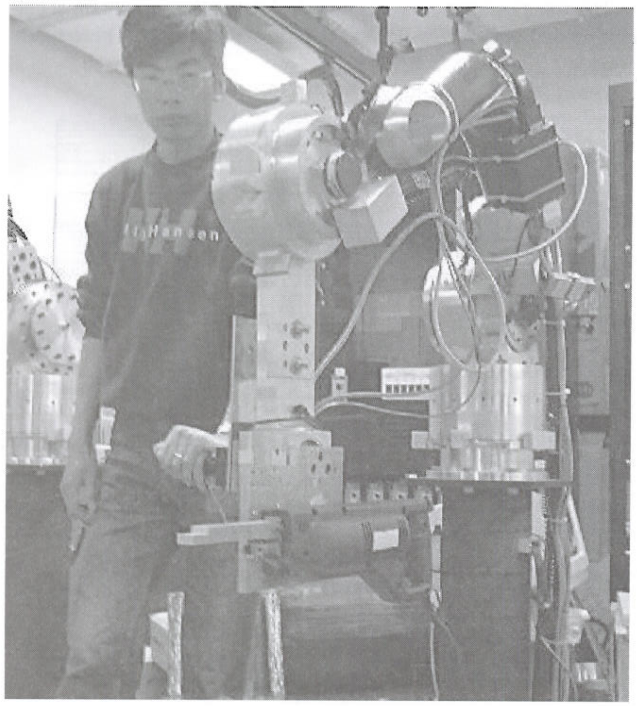

Fig. 18 The prototype extender

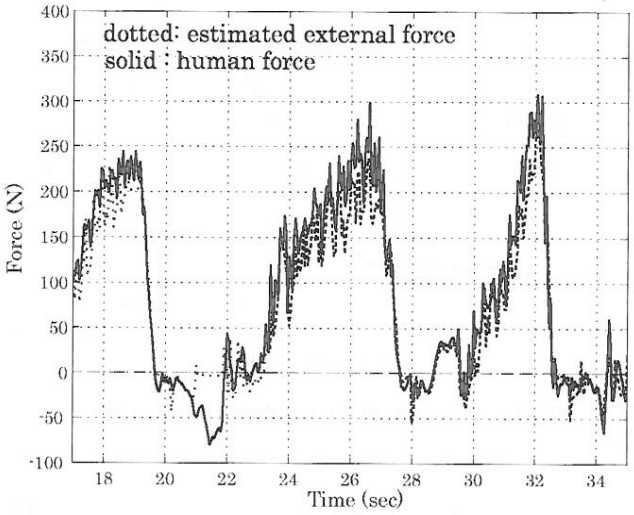

Fig. 19 Human/estimated force (spring)

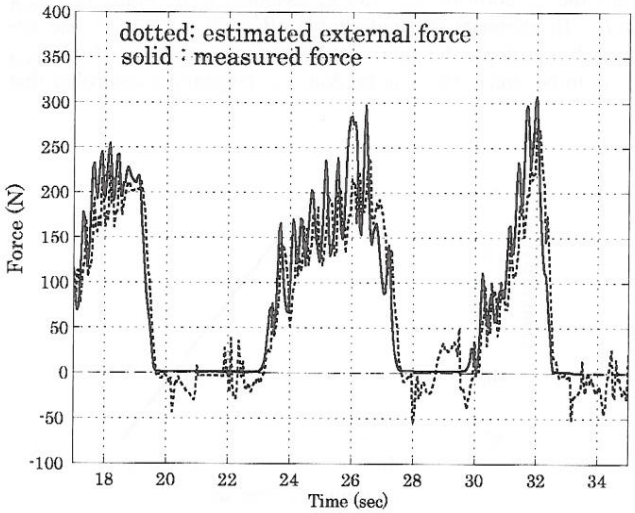

Fig. 20 Estimated/measured force (spring)

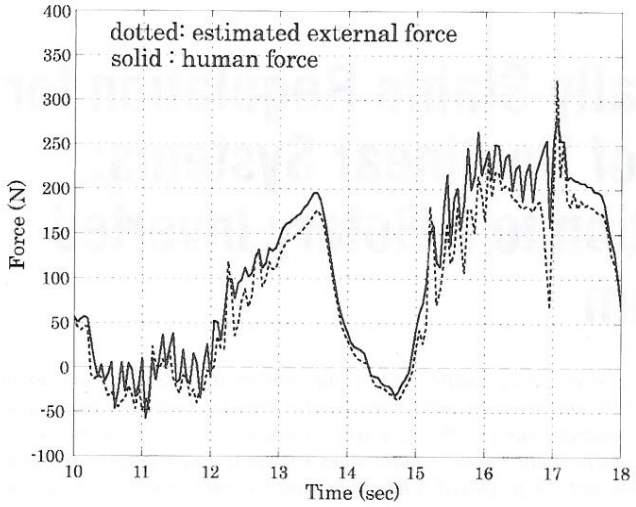

Fig. 21 Human/estimated force (wire)

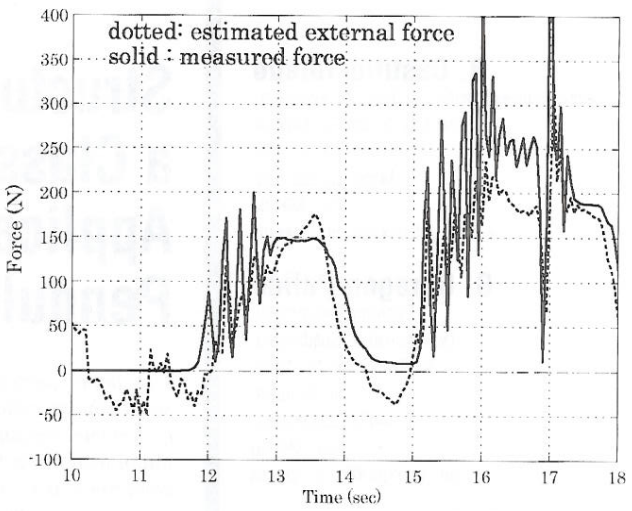

Fig. 22 Estimated/measured force (wire)

tender and the manipulation point near the grip an operator holds (cf. Fig. 10). Additionally, another force sensor is mounted on the end of the spring to verify the accuracy of the force estimation.

4.4.1 Spring Environment: Force Feedback Ratio α=0.1. Figure 19 shows the time response of the human force (solid line) and the estimated external force (dotted line) when force amplification filter is set on 0.1, i.e., the human force will be amplified 10 times. For convenience of comparison, the estimated force is magnified at 10 times.

Figure 20 shows a comparison of the estimated force and measured force (dashed line) to examine the accuracy of estimation.

4.4.2 Wire Environment: Force Feedback Ratio α=0.1. Figure 21 shows the time response of measured human force and estimated external force in the same manner as the previous case.

Figure 22 shows a comparison of the estimated force and measured force to examine the accuracy of estimation.

In both cases the estimation stayed within the tolerant range while the system was stable and error between the human force and the estimated external force is smaller than 10% of the magnitude of the human force, which proves that performance requirements were satisfied.

5 Conclusion

In this paper, we dealt with a system, which is subjected to very uncertain factors: human and environment. These independent uncertainties were dealt with explicitly based on μ-synthesis and a less conservative controller was obtained. We also developed a force sensorless control by taking into consideration the nonlinearly, such as, frictions and gravity force. A scaled down reaction force based on the estimation contributes compliant maneuvers. Finally, through experimental studies on the human power extender robot, stability and performance of the system were verified [8].

References

[1] Kazerooni, H., 1990, "Human Robot Interaction via the Transfer of Power and Information Signals," IEEE Trans. Syst. Man Cybern., **20**, pp. 450–463.
[2] Hollerbach, K., and Kazerooni, H., 1992, "Modeling Human Arm Movements Constrained by Robotic Systems," ASME Winter Annual Meeting, Advances in Robotics, DSC-Vol. 42, pp. 19–24.
[3] Doyle, J., Wall, J., and Stein, G., 1982, "Performance Robustness Analysis for Structured Uncertainty," in Proceedings of the 21st IEEE Confrence on Decision and Control, pp. 629–636.
[4] Doyle, J., 1985, "Structured Uncertainty in Control System Design," in Proceedings of the 24th IEEE Conference on Decision and Control, pp. 260–265.
[5] Doyle, J., Packard, A., and Zhou, K., 1991, "Review of LFTs, LMIs, and μ," in Proceedings of the 30th IEEE Conference on Decision and Control, Vol. 2, pp. 1227–1232.
[6] Chen, G., and Sugie, T., "An Upper Bound of μ Based on the Parameter Dependent Multipliers," in Proceedings of the IEEE American Control Conference, pp. 2604–2608.
[7] Bierman G., 1977. *Factorization Methods for Discrete Sequential Estimation*, Academic Press.
[8] Balas, G., Doyle, J., Glover, K., Packard, A., and Smith, R., "μ-Analysis and Synthesis Toolbox User's Guide," Mathworks, Natick, MA.